Observation of Supercurrent Enhancement in SNS Junctions by Nonequilibrium Injection into Supercurrent Carrying Bound Andreev States

Kutchinsky, Jonatan; Taboryski, Rafael J.; Sørensen, Claus Birger; Hansen, Jørn Bindslev; Lindelof, Poul Erik

Published in:
Physical Review Letters

Link to article, DOI:
10.1103/PhysRevLett.83.4856

Publication date:
1999

Document Version
Publisher's PDF, also known as Version of record

Observation of Supercurrent Enhancement in SNS Junctions by Nonequilibrium Injection into Supercurrent Carrying Bound Andreev States

Jonatan Kutchinsky,[1] Rafael Taboryski,[2] Claus B. Sørensen,[3] Jørn Bindslev Hansen,[1] and Poul Erik Lindelof[3]
[1]*Department of Physics, Technical University of Denmark, Building 309, DK-2800 Lyngby, Denmark*
[2]*Danish Institute of Fundamental Metrology, Anker Engelunds, Vej 1, DK-2800 Lyngby, Denmark*
[3]*Niels Bohr Institute, University of Copenhagen, Universitetsparken 5, DK-2100 Copenhagen, Denmark*
(Received 30 July 1999)

We report for the first time enhancement of the supercurrent by means of injection in a mesoscopic three terminal planar SN-SNS device made of Al on GaAs. When a current is injected from one of the superconducting Al electrodes at an injection bias $V = \Delta(T)/e$, the dc Josephson current between the other two superconducting electrodes has a maximum, giving evidence for an enhancement due to a nonequilibrium injection into bound Andreev states of the underlying semiconductor. The effect persists to temperatures where the equilibrium supercurrent has vanished.

PACS numbers: 74.50.+r, 73.23.–b, 85.25.–j

The study of nonequilibrium phenomena generated by current across superconductor-normal (SN) boundaries of superconductor-normal-superconductor (SNS) junctions has attracted much interest in recent years. It has been realized that supercurrents in SNS junctions are transmitted by the correlated electron-hole pairs generated by Andreev reflections at the SN boundaries. In this paper, we demonstrate experimentally a new supercurrent enhancement effect, where these correlated electron-hole pairs are affected by current injection across a third SN boundary.

In general, two effects have been studied in three terminal SNS devices. One is the field effect, where the carrier density in the normal region is controlled [1]. The other is injection, where the normal region is connected to one or two other reservoirs, biased with respect to the superconductor [2–4]. This modifies the quasiparticle energy distribution, either by simply increasing the electron temperature of the normal conductor, or by inducing a suitable nonthermal distribution function. These approaches are related to much older work [5], where superconductivity was enhanced close to T_c by redistributing quasiparticles by microwave irradiation or by tunneling resulting in an enhancement of the energy gap and other properties derived from this.

Recent theories for SNS junctions have predicted how injection can alter the Josephson coupling of the junction [6–8]. The supercurrent in the junction is carried by bound Andreev states, which in multichannel diffusive systems form a continuum. The role of a nonequilibrium electron distribution can be seen if one considers this spectral distribution N_j of supercurrent carrying states [6], together with the energy distribution of electrons f in the normal conductor. From these the supercurrent as a function of the phase difference between the superconductors can be written:

$$I_s(\phi) = -2ev_F A \int_0^\infty d\varepsilon N_j(\varepsilon, \phi)[f(-\varepsilon) - f(\varepsilon)], \tag{1}$$

where A is the cross section of the conductor. The energy ε is defined with respect to the chemical potential of the superconductors. In equilibrium f is the Fermi distribution function. The distribution N_j depends on the sample geometry, and can for simple systems be calculated directly from quasiclassical Green's function theory [6,7]. In diffusive systems N_j varies on the scale of the Thouless-energy $\varepsilon_L = \hbar D/L^2$, where D is the diffusion constant and L is the distance between the superconductors. For long junctions where $\Delta \gg \varepsilon_L$ (Δ is the superconductor energy gap), N_j peaks at $\varepsilon \approx \varepsilon_L$. In equilibrium the critical supercurrent decay with the normal conductor coherence length $\xi_N(T) = \sqrt{\hbar D/2\pi k_B T}$. For long junctions [9]

$$I_c = I_0 \frac{\Delta^2(T)}{\Delta^2(0)} \sqrt{\frac{T_c}{T}} \exp[-L/\xi_N(T)], \tag{2}$$

where $I_0 = 8\Delta^2(0)L/(eR_N\sqrt{2\pi\hbar D k_B T_c})$, and R_N is the junction normal resistance. If, however, the distribution function contains a sharp feature, narrower than $k_B T$, at the energies where the supercurrent-carrying states are present, a very different temperature dependence and even a change of sign can be expected.

In the Baselmans experiment [4] the nonequilibrium distribution function had the form of a thermally rounded step function comprised of a linear combination of two mutually bias-displaced Fermi functions of the normal reservoirs at each end of the filamentary normal conductor. The observed effect was, however, much weaker than the equilibrium supercurrent (without injection). A considerably stronger effect can be anticipated if the relevant nonequilibrium distribution function derived from the thermally rounded Fermi functions of the normal reservoirs is replaced by a distribution function induced between two voltage biased superconducting reservoirs. If the size of the normal conductor is smaller than the phase-breaking diffusion length, the nonequilibrium electron energy distribution in the normal conductor will contain a replica of the

 0031-9007/99/83(23)/4856(4)$15.00

sharp singularities in the superconducting density of states of the reservoirs. The fingerprints of these are seen as a subgap structure in the I-V characteristics of SNS junctions [10]. At a bias voltage of $V = \Delta(T)/e$ the singularities in the normal conductor distribution function match the Fermi energies of the superconductors, where the supercurrent carrying states are concentrated. The resulting injection induced supercurrent in the adjacent SNS junction is thus expected to have a maximum for an injection bias $V = \Delta(T)/e$, and a weak temperature dependence due to the small thermal smearing of the distribution function in play. Besides these nonequilibrium effects a broad heating effect is expected, which will always suppress the critical supercurrent.

In this Letter we demonstrate experimentally for the first time that the superconductivity of an SNS junction can be enhanced above the equilibrium value by injecting quasiparticles with an energy distribution which matches the spectral supercurrent density $N_J(E)$. The effect is realized in a three terminal sample geometry, where three superconducting Al electrodes are connected to the same piece of highly doped GaAs semiconductor. One of the electrodes is used as a common ground for the current flow. Another electrode is used as a detector and the third electrode as an injector. For the particular devices studied we find that the injection-induced supercurrent exceeds the equilibrium supercurrent at temperatures above 0.6 K (approximately $\frac{1}{2}T_c$).

The samples were formed from a layered structure of GaAs and Al, grown in an MBE chamber. Here, 200 nm of highly doped n-GaAs were grown on an undoped/insulating substrate. This was then capped with 150–200 nm Al. In order to reduce the Schottky barrier between GaAs and Al, five layers of δ doping with 5×10^{13} cm^{-2} Si were inserted in the GaAs just below the Al. The Al film was subsequently deposited without breaking the vacuum. This resulted in a contact resistance of $8 \times 10^{-9}\ \Omega\,\text{cm}^2$. Samples with a planar geometry as shown in Fig. 1 were then formed by removing Al in selected areas with conventional E-beam lithography and wet etch. Larger scale patterning to form a 20 μm wide mesa structure was done with UV lithography. The details of the fabrication have been published elsewhere [11].

The measurements were performed in a pumped ^{3}He cryostat with a base temperature of 235 mK. At low temperatures the GaAs-film had a carrier density of $n = 5.5 \times 10^{18}$ cm^{-3} and a mean free path of $\ell = 42$ nm, corresponding to a diffusion constant $D = 127$ cm^2/s. In an independent weak localization experiment the phase-breaking diffusion length was found to be $\ell_\phi \approx 5$ μm at the base temperature. The Al film had a superconducting critical temperature of 1.196 K. All measured samples had nearly identical characteristics. The data presented in this paper are based on a single sample, although all samples exhibited similar effects. This particular sample is shown in Fig. 1.

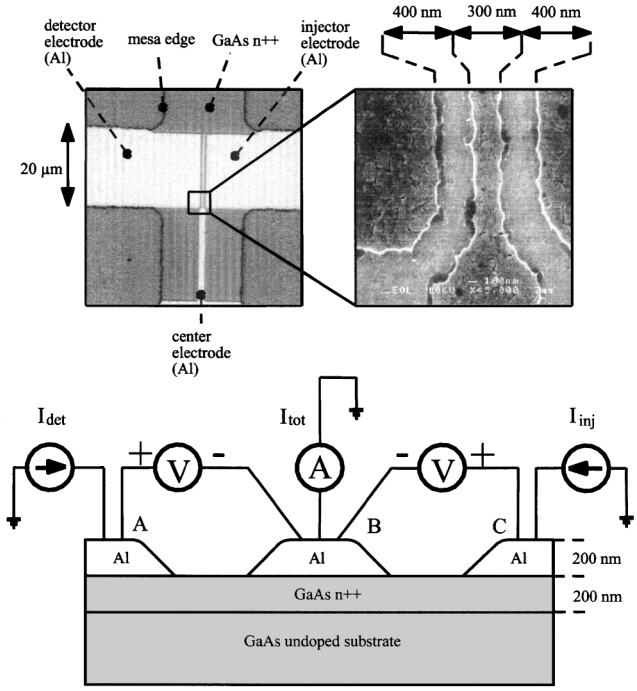

FIG. 1. The three terminal device and the measurement setup. Top panel: Optical photograph of the sample, with SEM close-up. Both seen from above. The bright areas consist of Al, the darker GaAs. The SEM picture shows the roughness of the Al edge, due to the crystal grain boundaries. Bottom: Schematic cut-through of the sample, with measurement leads indicated. The injector and detector currents were controlled by high-impedance current sources. The middle lead (output) was connected to ground. The output current I_{out} was measured to make sure there were no leaks or nonlinearities in the setup. The voltages V_{inj} and V_{det} were measured through separate leads to the superconducting electrodes.

The three superconducting Al electrodes are connected to the same piece of GaAs within mesoscopic range. The distance between two neighboring electrodes is approximately 400 nm corresponding to a Thouless-energy $\varepsilon_L = 52$ μeV. The junctions AB and BC formed individual Josephson junctions with normal resistances 3.3 and 3.2 Ω, and critical currents respectively 2.2 and 3.4 μA at 240 mK, when all electrodes were kept at zero voltage. The junction AC was much weaker coupled because of the longer distance between A and C. In this experiment we define the AB junction as the detector, and the BC junction as the injector. The critical supercurrent was measured on the detector, while the injector was biased at high voltages. Because the samples were symmetrical, the roles of the two junctions could be (and were) interchanged. During the experiment, a detector current was passed through electrode A, and an injection current was passed through electrode C, both from high impedance (470 kΩ) dc current sources. Electrode B was connected to ground through an ammeter, in order to check that no current leaks were present in the setup. The detector (AB) and injector (BC) voltages were measured

by separate leads to the superconductors. All leads to the sample were fitted with 50 cm low temperature THERMOCOAX filters providing high frequency power attenuation of $12.5\sqrt{f[\mathrm{GHz}]}$ dB and room temperature π filters giving approximately 20 dB attenuation at 700 kHz.

Both the detector and injector junctions showed a "Fraunhofer" type of pattern with up to 10 well-developed lobes in the critical supercurrent vs applied magnetic field, indicating a high degree of homogeneity of the junctions. Before each measurement series on the 3-terminal samples, the magnetic field was carefully zeroed to within a small fraction of a flux quantum [12].

In Fig. 2 we show the detector supercurrent at various injection currents. In the left panel, the detector critical current I_c is plotted as a function of the injection current at three different temperatures. Above the highest injection currents shown in the figure, the central electrode suddenly went normal due to a current in excess of its critical current and above this, injector bias measurements could not be made. Each data point is the result of a fit to a noise rounded resistively shunted junction (RSJ) model [13] of individual I-V characteristics of the detector junction. In the right panel of Fig. 2 we show three examples of the fits. The injection currents and fitted I_c of these are indicated with arrows in the left panel. The fitted noise temperature varied randomly in the range 1–3 K due to the error on the measured data [14]. The I-V characteristics of the detector junction show current offsets. The offsets are simply a fraction of the injector current and are exclusively due to the sample geometry, where the three electrodes are connected to the same piece of GaAs. Consequently, the detector current I_{det} has to be compensated by about one fourth of the injection current for the detector to be at zero bias.

In the left panel of Fig. 2, we see that the critical supercurrent exhibits two clear features as a function of injection current (and voltage). The equilibrium supercurrent appears to be falling off rapidly with increasing injection current, and is seen to be strongly temperature dependent. The next maximum appearing for higher injection currents is interpreted as a nonequilibrium supercurrent. At very high injection currents, close to the critical current of the central electrode, we observe a weak enhancement of the critical current. This effect remains unexplained. The nonequilibrium critical current builds up with increasing injection current to a maximum (at 400 mK indicated by C in Fig. 2). We see that while the equilibrium supercurrent is dominating at 400 mK, at 900 mK it has almost vanished. The nonequilibrium supercurrent, on the other hand, is almost temperature independent [15], and by far exceeds the equilibrium supercurrent at 900 mK. At 600 mK the two critical currents have equal magnitude. Although in the figure we mostly plot the properties for positive injection currents, we would like to emphasise that the effect was completely symmetrical upon reversal of current direction. The effects were reproduced in several samples.

In Fig. 3 we show a detailed plot of the temperature dependence of both the critical current at zero injection, and the optimal nonequilibrium current. The detector I_c without injection (squares) has a strong temperature dependence, which has been fitted to Eq. (2) with parameters $I_0 = 4.9\ \mu$A and $\xi_N(T_c) = 115$ nm. From the independently measured sample parameters we find $I_0 = 363\ \mu$A and $\xi_N(T_c) = 113$ nm. The large deviation of the prefactor I_0 may be attributed to the fact that the calculation of Eq. (2) does not take interface barriers into account.

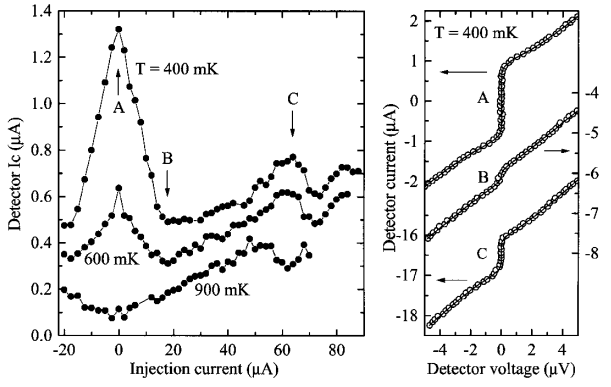

FIG. 2. The detector supercurrent at various injection currents. Left panel: The detector critical currents I_c plotted as a function of the injection current at three different temperatures. The data for $T = 600$ and 400 mK have been shifted upwards with 0.1 and 0.2 μA, respectively. Right panel: The I/V characteristics of the detector at 400 mK and (A) no injection, (B) 18 μA injection, and (C) 64 μA injection. Circles represent measurements. The curves represent fits to the RSJ model. The three plots have separate y axes indicated by the arrows.

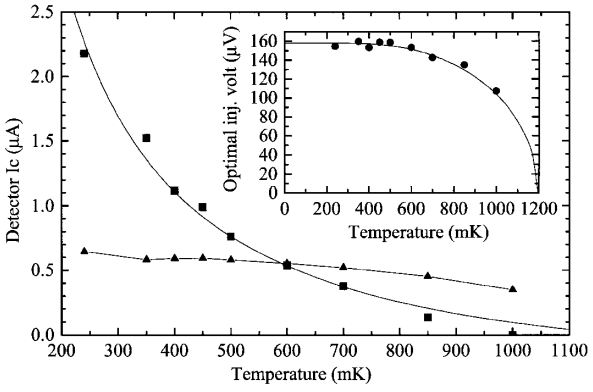

FIG. 3. The critical supercurrent I_c of the detector junction as a function of temperature. Squares: I_c with no injection. Triangles: nonequilibrium supercurrent I_c at the optimal injection current for a given temperature. The curve through the no-injection points is a fit with Eq. (2). To guide the eye, lines connect the optimal injection data points. Inset: Circles indicate the optimal injector voltage for a given temperature. The curve shows the BCS theory gap function.

The other curve (triangles) shows the maxima of the injection induced nonequilibrium I_c as exemplified for three temperatures in Fig. 2. This only decreases slightly with increasing temperature. In the inset, we plot the corresponding voltage across the injector junction for each of these points. The injector voltage varied slightly during each detector I-V measurement. The plotted value was taken where the detector current I_{det} matched the earlier mentioned current offset. The full curve in the inset shows the BCS theory gap function, where $T_c = 1.196$ K has been measured, and $\Delta(0) = 158\ \mu$eV has been adjusted from the bulk value 175 μeV to fit the data. It is clearly seen that the injection bias giving the maximum nonequilibrium supercurrent, corresponds to the superconductor energy gap $\Delta(T)$. Together with the weak temperature dependence of the nonequilibrium critical current, we take this as the most important experimental indication that the observed injection induced phenomena are related to a nonequilibrium population of the supercurrent carrying states. This nonequilibrium population is induced by Andreev reflections on the superconducting injection electrode, and is possessing a sharp kink at the superconducting gap energy. This kink originates from the singularities in the density of states of the superconductor. The functional dependence of the spectral supercurrent density of Eq. (1) has not been calculated for the planar geometry of the samples used in the experiment; however, the form of the distribution function may allow us to probe the varying part of N_j. We believe the observed phenomena are related to the earlier observations published in Ref. [16], where a maximum in oscillation amplitude in a flux sensitive interferometer was observed for the bias voltages $V = \Delta/e \pm \varepsilon_L$. Here the phase dependent (coherent) change of the normal resistance was probed instead of the supercurrent.

In conclusion, we have measured the injection-induced supercurrent in a three terminal device. Above 600 mK the induced nonequilibrium supercurrent exceeds the equilibrium (zero injection) supercurrent. The optimal injection induced critical current is observed when the injector electrode is biased at $V = \Delta(T)/e$. Further studies are needed to map out the detailed properties of the nonequilibrium supercurrent, e.g., the magnetic field dependence and the dc Josephson effects.

We acknowledge useful discussions with Vitaly Shumeiko and Jonn Lantz. We thank the III-V Nanolab of the Niels Bohr Institute for providing the processing facilities. This work has been supported by the Danish Technical Research Council, and the Velux Foundation.

[1] T. Akazaki, H. Takayanagi, J. Nitta, and T. Enoki, Appl. Phys. Lett. **68**, 418 (1996).
[2] Th. Schäpers *et al.,* Appl. Phys. Lett. **73**, 2348 (1998).
[3] A. F. Morpurgo, T. M. Klapwijk, and B. J. van Wees, Appl. Phys. Lett. **72**, 966 (1998).
[4] J. J. A. Baselmans, A. F. Morpurgo, B. J. van Wees, and T. M. Klapwijk, Nature (London) **397**, 43 (1999).
[5] For a review, see J. E. Mooij, in *Nonequilibrium Superconductivity, Phonons, and Kapitza Boundaries,* edited by K. E. Gray (Plenum, New York, 1981).
[6] S.-K. Yip, Phys. Rev. B **58**, 5803 (1998); F. Wilhelm, G. Schön, and A. D. Zaikin, Phys. Rev. Lett. **81**, 1682 (1998).
[7] A. F. Volkov and H. Takayanagi, Phys. Rev. B **56**, 11 184 (1997); A. F. Volkov and V. V. Pavlovskii, JETP Lett. **64**, 670 (1996).
[8] P. Samuelsson, V. S. Shumeiko, and G. Wendin, Phys. Rev. B **56**, 5763 (1997); P. Samuelsson, J. Lantz, V. S. Shumeiko, and G. Wendin, cond-mat/9904276.
[9] K. K. Likharev, Rev. Mod. Phys. **51**, 101 (1979).
[10] M. Octavio, M. Tinkham, G. E. Blonder, and T. M. Klapwijk, Phys. Rev. B **27**, 6739 (1983); K. Flensberg, J. Bindslev Hansen, and M. Octavio, Phys. Rev. B **38**, 8707 (1988).
[11] R. Taboryski *et al.,* Appl. Phys. Lett. **69**, 656 (1996).
[12] The magnetic field created by the injection current is negligible in comparison with one flux quantum through the junction area.
[13] V. Ambageokar and B. I. Halperin, Phys. Rev. Lett. **22**, 1364 (1969).
[14] The RSJ model assumes white noise. Our experimental setup is, however, dominated by noise below 1 kHz. The extracted noise temperature is therefore not the electron temperature in the device, but rather represents external low-frequency noise.
[15] The highly nonequilibrium condition of the experiment makes it difficult to define an electron temperature in the active normal conducting region. Since the inelastic scattering length is much longer than this region, the thermalization of the electrons mainly takes place in the superconducting electrodes, far from the junction compared with the length scales relevant for Andreev scattering.
[16] J. Kutchinsky *et al.,* Phys. Rev. Lett. **78**, 931 (1997); Phys. Rev. B **56**, 2932 (1997); R. Taboryski *et al.,* Superlattices Microstruct. **25**, 829 (1999).